Supporting information to

Surface Effect of Alumina on the First Electronic Transition of Liquid Water Studied by Far-Ultraviolet Spectroscopy

Authors names: Takeyoshi Goto,[I*] Akifumi Ikehata,[II] Yusuke Morisawa,[III] and Yukihiro Ozaki[I]

Affiliations: [I] Department of Chemistry, School of Science and Technology, Kwansei Gakuin University, Sanda, Hyogo 669-1337, Japan

[II] National Food Research Institute, National Agriculture and Food Research Organization (NARO), Tsukuba, Ibaraki 305-8642, Japan

[III] Department of Chemistry, School of Science and Engineering, Kinki University, Higashi-Osaka, Osaka 577-8502, Japan

This file includes 4 sections of supporting information. Reference numbers are those used in the main text.

(1) Kramers-Kronig transformation of the measured ATR-FUV spectra

(2) VA spectral analysis

(3) Figure S1

(4) Tables S1

Kramers-Kronig transformation of the measured ATR-FUV spectra

The detailed procedure of Kramers-Kronig transformation (KKT) for an ATR-FUV spectrum is described in the reference 5. In order to apply the KKT, the measured ATR-FUV spectra were extrapolated from 142 to 120 nm by nonlinear least squares fit modeled with Gaussian shapes based on Heller's optical constants of water.[34] We employed the real part of refractive index at 589.0 nm as one in the high frequency limit (n_∞); 1.333 and 1.329 for H_2O and D_2O, respectively.

VA spectral analysis

The measured VA spectra contain information about the electronic transition of water molecules positioned at various depths from the alumina surface according to θ. The degree to which the electric fields of the probe light can spatially interact with water molecules along the z direction can be represented from the two physical lengths: penetration depth (d_p) and effective thickness (d_e).[19] The penetration depth, defined as the distance required for the electric field intensity to be attenuated to 1/e at the surface, is given by:

$$d_p(\lambda) = \frac{\lambda}{2\pi n_p(\sin^2\theta - (n_s/n_p)^2)^{1/2}} \qquad (1),$$

where λ is the wavelength of the probe light, and n_p and n_s are the refractive indices of the alumina prism and sample, respectively. The n_p values were obtained from the reference 35 and the n_s values were obtained by KKT calculation of the measured spectra. The effective thickness represents the coupling strength of the evanescent wave to the sample:

$$d_{e\perp}(\lambda) = \frac{\lambda(n_s/n_p)\cos\theta}{\pi n_p(1-(n_s/n_p)^2)(\sin^2\theta - (n_s/n_p)^2)^{1/2}} \qquad (2)$$

$$d_{ell}(\lambda) = \frac{\lambda(n_s/n_p)\cos\theta(2\sin^2\theta - (n_s/n_p)^2)}{\pi n_p(1-(n_s/n_p)^2)(\sin^2\theta - (n_s/n_p)^2)^{1/2}[(1+(n_s/n_p)^2)\sin^2\theta - (n_s/n_p)^2]} \qquad (3)$$

$$d_e(\lambda) = \frac{d_{e\perp} + d_{ell}}{2} \qquad (4).$$

To be more specific, d_p corresponds to the distance at which the electric fields of the probe light penetrate into liquid water from the alumina surface and d_e to the pathlength at each θ. In the present VA spectral analysis, the mean values of d_p and d_e in the wavelength region 140–180 nm (8.86–6.89 eV), in which the $\tilde{A} \leftarrow \tilde{X}$ band of liquid water was observed, were employed. As θ becomes larger from 58.4° to 71.8°, d_p decreases from 25 to 19 nm, and d_e from 94 to 43 nm. The d_p and d_e values with θ are listed in Table S1.

The individual FUV spectra of liquid water contributed from the bulk phase (d_p > 2 nm) and interfacial phase (<2 nm) were determined by linearly decomposing the measured VA spectra into an absorption coefficient spectrum (α) and a pathlength (l) of each phase, based on Lambert's law:

$$\mathbf{A} = \boldsymbol{\alpha}_{\mathbf{bulk}}\mathbf{l}_{\mathbf{bulk}} + \boldsymbol{\alpha}_{\mathbf{interf.}}\mathbf{l}_{\mathbf{interf.}} \qquad (5)$$

where **A** is absorbance matrix (wavelength (λ) × incident-angle (θ) channels), calculated from the product of α and d_e values at each θ. An alternating least square (ALS) calculation determined the compromise solutions of the absorption coefficient matrix (**α**, λ × number of phases (n = 2)) and the pathlength matrix (**l**, $l \times n$) using the initial **l** matrix. In order to apply the equation (5), the effective pathlength of the interfacial phase ($l_{interf.}$) was defined as (d_e/d_p) × 2 nm, which converted the d_p based interfacial distance 2 nm to the d_e based distance. We employed the mean values of $l_{interf.}$ for all the incident angles; 6.12 nm and 6.09 nm for H_2O and D_2O, respectively. The initial **l** matrix comprised the effective pathlength of the bulk phase ($l_{bulk} = d_e - l_{interf.}$) and interfacial phase ($l_{interf.}$) at each θ.

Figure S1 shows the imaginary part of the refractive index (k) of liquid water of the variable angle (VA) spectra (58.4º and 71.8º), the bulk water, and the literature spectra from the references 1 and 3. The VA spectra appeared the higher photon energy region than the reported bands with external reflection (Painter, 1968) and transmission (Sowers, 1972) methods. This indicates that an ATR spectrum in the FUV region represented the interfacial phase more strongly due to the short penetration depth of the evanescent wave than the other methods. The decomposed band of the bulk water appeared in the lower region than the transmission spectrum, which might reflect the surface effect of the transmission optical cell.

(34) Heller, J. M. Collective Oscillation in Liquid Water. *J. Chem. Phys.* **1974**, *60*, 3483–3486.

(35) D. B. Leviton, T. J. Madison, and P. Petrone III, Far Ultraviolet Refractive Index of Optical Materials for Solar Blind Channel (SBC) Filters for HST Advanced Camera for Surveys. *SPIE Proc.* **1998**, *3425*, 219–230.

Figure S1: The imaginary part of the refractive index (k) of liquid water of the variable angle (VA) spectra (58.4º and 71.8º), the bulk water, and the literature spectra from the references 1 and 3.

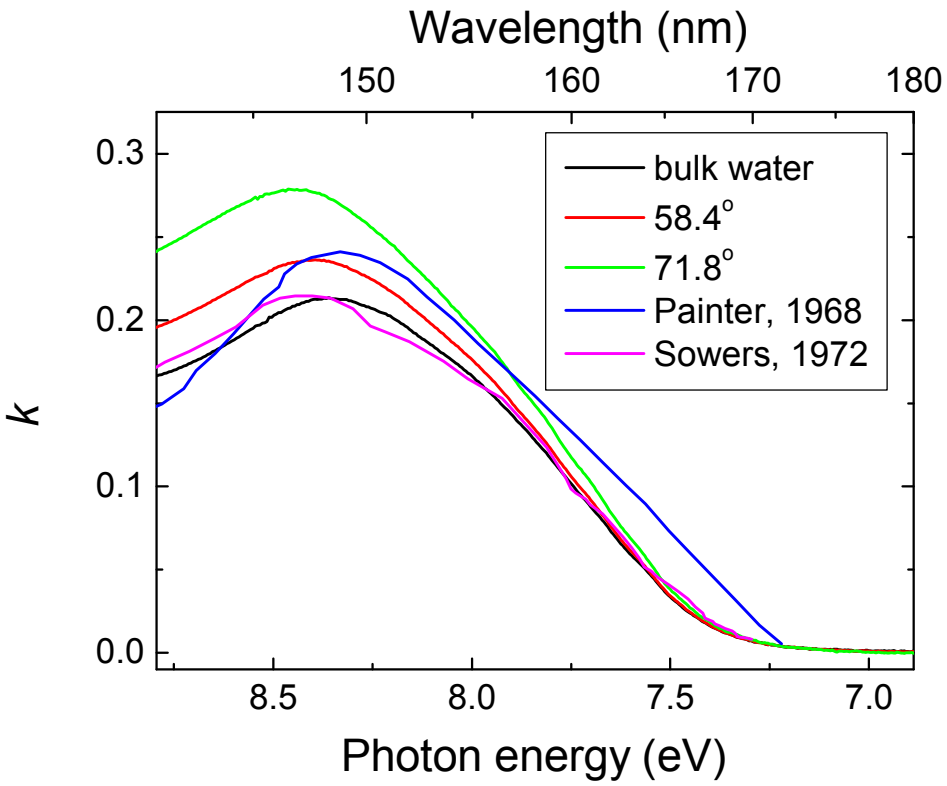

Table S1: Variations of effective thickness (d_e, nm) and penetration depth of evanescent field (d_p, nm) with incident angles (θ, degree). Values of d_e and d_p are means in the wavelength region 140–180 nm.

	H_2O		D_2O	
θ	d_e	d_p	d_e	d_p
58.4	94.45	24.96	93.50	24.84
60.0	86.73	23.94	85.78	23.83
61.1	81.87	23.33	81.15	23.24
62.2	76.82	22.71	76.15	22.63
63.8	69.69	21.88	69.13	21.81
65.4	63.59	21.20	63.11	21.14
67.0	57.58	20.56	57.25	20.52
68.6	52.63	20.08	52.39	20.05
70.2	47.99	19.66	47.72	19.62
71.8	43.49	19.27	43.32	19.25